



# Interplay between Angular-Dependent Magnetoresistance Oscillation and Charge-Ordered States in the Organic Conductor $\beta''$ -(ET)(TCNQ)

Syuma Yasuzuka<sup>1,2\*</sup>, Shinya Uji<sup>3</sup>, Taichi Terashima<sup>3</sup>, Takako Konoike<sup>3</sup>, David Graf<sup>4</sup>, Eun Sang Choi<sup>4</sup>, James S. Brooks<sup>4†</sup>, Hiroshi M. Yamamoto<sup>5,6</sup>, and Reizo Kato<sup>5</sup>

<sup>1</sup>Research Center for Applied Quantum Physics, Hiroshima Institute of Technology, Hiroshima 731-5193, Japan

<sup>2</sup>National Institute for Materials Science (NIMS), Tsukuba, Ibaraki 305-0003, Japan

<sup>3</sup>Research Center for Materials Nanoarchitectonics (MANA), National Institute for Materials Science (NIMS), Tsukuba, Ibaraki 305-0003, Japan

<sup>4</sup>National High Magnetic Field Laboratory, Florida State University, Tallahassee, FL 32310, U.S.A.

<sup>5</sup>Condensed Molecular Materials Laboratory, RIKEN, Wako, Saitama 351-0198, Japan

<sup>6</sup>Research Center of Integrative Molecular Systems, Institute for Molecular Science, Okazaki, Aichi 444-8585, Japan

(Received June 1, 2024; revised June 26, 2024; accepted July 9, 2024; published online August 28, 2024)

In this paper, we report on the effect of pressure on the angular-dependent magnetoresistance and Shubnikov–de Haas (SdH) oscillation for  $\beta''$ -(ET)(TCNQ), where ET and TCNQ stand for bis(ethylenedithio)tetrathiafulvalene and tetracyanoquinodimethane, respectively. At 0 kbar, the temperature dependence of the interlayer resistance shows three hump anomalies at around  $T_1 = 174$  K,  $T_2 = 72$  K, and  $T_3 = 22$  K. At low temperatures below  $T_3$ , both the Yamaji oscillation and the periodic dip structure due to a commensurability effect are clearly observed in the angular dependence of the interlayer resistance at high magnetic fields. At 2.0 kbar, the  $T_1$ -anomaly is suppressed and the  $T_2$ - and  $T_3$ -anomalies shift to lower temperatures. Below  $T_3$ , a similar Yamaji oscillation and the dip structure are evident. At 5.1 kbar, the  $T_3$ -anomaly is removed, and only the dip structure is clearly observed at low temperatures. From this finding, the dip structure is attributable to a commensurability effect between the possible  $4k_F$  charge-density wave in the TCNQ layers and the interlayer lattice potential. Although no Yamaji oscillation is observed at 5.1 kbar, a higher SdH frequency than that at 0 kbar is detected, suggesting the emergence of a magnetic breakdown orbit in the significantly undulated Fermi surface originating from the ET layers. The temperature–pressure phase diagram of  $\beta''$ -(ET)(TCNQ) is determined from the resistance measurements.

## 1. Introduction

Layered organic conductors, which are often regarded as strongly correlated electron systems, have provided various interesting electronic states. Examples include charge- and spin-density waves (CDWs and SDW, respectively), the charge ordering (CO) state driven by electron correlations, and unconventional superconductivity.<sup>1–8</sup> Reflecting softness arising from the van der Waals nature of molecular packing, these electronic states can be controlled by applying moderate pressure.<sup>7–18</sup> To well understand such physical properties, their Fermi surfaces (FSs) have been intensively studied by various techniques, e.g., quantum oscillations [de Haas–van Alphen (dHvA) or Shubnikov–de Haas (SdH) effect], periodic orbit resonance, angle-resolved photoelectron spectroscopy, and angular-dependent magnetoresistance oscillation (AMRO).<sup>6,19–29</sup>

In this paper, we report on the effect of pressure on the angular-dependent magnetoresistance and SdH oscillation of the quarter-filled layered organic conductor  $\beta''$ -(ET)(TCNQ), where ET and TCNQ stand for bis(ethylenedithio)tetrathiafulvalene and tetracyanoquinodimethane, respectively.<sup>30,31</sup> The crystal structure has triclinic symmetry consisting of ET and TCNQ layers, and there exist one ET and one TCNQ in the unit cell, as schematically depicted in Fig. 1(a).<sup>30,31</sup> According to the band structure calculation, a highly one-dimensional (1D) band of TCNQ stacked along the  $c$ -axis and a warped 1D band of ET extended along the  $a$ -axis are formed. Thus, the FSs with rectangular cross sections, originally formed by two pairs of orthogonal 1D FSs, are predicted as shown in Fig. 1(b).<sup>30,31</sup>

The temperature dependence of the resistivity of  $\beta''$ -(ET)(TCNQ) is found to exhibit metallic behavior with three

hump anomalies at  $T_1 \sim 175$  K,  $T_2 \sim 80$  K, and  $T_3 \sim 20$  K.<sup>30,31</sup> Optical spectroscopy and X-ray scattering studies revealed a checkerboard pattern of the CO state in the ET layer at room temperature.<sup>32,33</sup> Interestingly, this CO state disappears below  $T_1$ ,<sup>32,33</sup> where the magnetic susceptibility also shows a kink.<sup>31</sup> According to the optical conductivity measurement,<sup>33,34</sup> the coherence of the quasiparticle in the ET layer increases monotonically below  $T_1$ , and the electronic state in the ET layer finally behaves as a metal with a Fermi liquid nature below  $T_3$ , where several 2D SdH frequencies were observed. Below  $T_3$ , the magnetic susceptibility shows a sharp drop and is independent of the magnetic field direction.<sup>30,31</sup> Thus, the resistivity anomaly at  $T_3$  may be related to a density wave (DW) transition driven by an imperfect nesting of the FSs originating from the ET bands. In fact, an X-ray scattering study<sup>35</sup> has revealed new satellite reflections with a modulation vector.

On the other hand, the vibronic bands are observed in the optical conductivity polarized parallel to the TCNQ stacking direction (i.e.,  $c$ -axis) at 280 K, and no additional vibronic bands are found down to 6 K.<sup>33,34</sup> This observation suggests a  $4k_F$  lattice modulation in the TCNQ layers below room temperature. Although the formation of a  $4k_F$ -CDW and the annihilation of the FSs originating from the TCNQ band are expected, the electronic state in the TCNQ layers is not well characterized in the infrared and Raman studies.<sup>32–34</sup>

Below  $T_3$ , measurements of the AMRO were performed extensively by the authors.<sup>27</sup> The AMRO consists of long- and short-period oscillations. The long-period oscillation is ascribed to the Yamaji oscillation corresponding to the small FS pocket labeled  $\alpha$ -orbit [see Fig. 1(b)].<sup>27,36</sup> The Yamaji oscillation arises from the orbital motion of the electrons on the corrugated cylindrical FS.<sup>24</sup> The peaks in the Yamaji

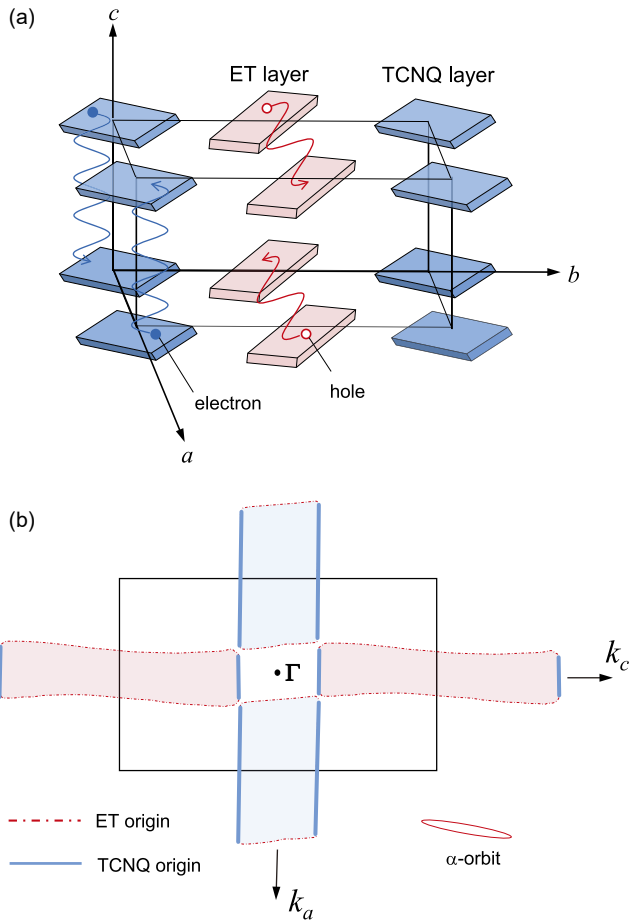


**Fig. 1.** (Color online) (a) Schematic of crystal structure of  $\beta''$ -(ET)(TCNQ). (b) Calculated FS of  $\beta''$ -(ET)(TCNQ), where the FSs originating from the ET and TCNQ layers are indicated by the dashed and solid curves, respectively.<sup>30,31</sup> The FS pocket labeled  $\alpha$ -orbit in the same scale as the first Brillouin zone is shown on the bottom right side.

oscillation appear when the averaged electronic group velocity along the interlayer direction vanishes as the field is tilted. For a simply corrugated cylindrical FS, the peaks appear periodically as a function of  $\tan \theta$ , where  $\theta$  is the angle between the magnetic field and the least conducting axis. The shape of the  $\alpha$ -orbit is found to be strongly elongated approximately along the  $c$ -axis, in agreement with previous magneto-optical measurements.<sup>37</sup> Judging from the shape of the FS, the  $\alpha$ -orbit may be generated by the imperfect nesting of the FSs originating from the ET layers.

The short-period oscillation, the periodic behavior of the resistance dips rather than the peaks, has been discussed in terms of the Yoshioka model.<sup>38</sup> When a periodic potential with wave vector  $\mathbf{Q}$  is turned on by DW formation, the additional scattering of the carriers by the double periodicity (lattice and DW) increases the interlayer resistance. However, this scattering effect is suppressed when the magnetic field direction satisfies a commensurability condition depending on  $\mathbf{Q}$ . This commensurability effect leads to periodic dips as a function of the field angle. On the basis of the Yoshioka model,<sup>38</sup> the superlattice vector  $\mathbf{Q}$  is found to be nearly parallel to the  $c$ -axis. One of the DWs from the ET band or the possible  $4k_F$ -CDW from the TCNQ band will be the origin of the dip structures.<sup>27</sup> However, it remains an open question as to which band plays a decisive role.

To further investigate the electronic state, we have performed the measurements of the angular-dependent magnetoresistance under pressure for  $\beta''$ -(ET)(TCNQ) since the pressure could selectively suppress the superlattice potentials associated with the DW and possible  $4k_F$ -CDW.<sup>39,40</sup> In this paper, we will show that the angular-dependent magnetoresistance is drastically changed by the pressure. In addition, a high-frequency SdH oscillation above 30 T is observed at 7.0 kbar, indicating a significant difference between the FSs at 0 and 7.0 kbar. The temperature–pressure phase diagram of  $\beta''$ -(ET)(TCNQ) is determined from the resistance measurements. These results reveal an important interplay between the electronic state and pressure in  $\beta''$ -(ET)(TCNQ).

## 2. Experimental

To obtain single crystals of  $\beta''$ -(ET)(TCNQ), a  $\text{CH}_2\text{Cl}_2$  (or  $\text{CH}_2\text{Br}_2$ ) solution of ET, TCNQ, and TIE (= tetraiodoethylene) was placed at room temperature, and the solvent was allowed to evaporate slowly to dryness within 24 h.<sup>30,31</sup> The interlayer resistance was measured by a conventional four-probe AC technique with electric current along the  $b^*$ -axis (the least-conducting axis). Pressure was generated using a WC piston and a beryllium-copper clamp type cylinder. Daphne 7373 oil was used as a pressure-transmitting liquid.<sup>41</sup> The pressures were calibrated from the  $\text{NH}_4\text{F}$  I–II transition at room temperature. Since the pressure decreases by about 1.5 kbar between room temperature and 200 K,<sup>41</sup> the pressure shown here is reduced by 1.5 kbar from the value at room temperature. The clamped pressure cell with samples inside was rotated in the  $b^*$ - $c$  plane using a single-axis rotator. The angle  $\theta$  is the angle between the magnetic field and the least-conducting  $b^*$ -axis within the  $b^*$ - $c$  plane. The experiments were carried out using a  $^4\text{He}$  cryostat with a 15 T superconducting magnet at the National Institute for Materials Science, Tsukuba, Ibaraki, Japan. Higher magnetic field experiments were performed in a 33 T resistive magnet at the National High Magnetic Field Laboratory, Tallahassee, Florida.

## 3. Results and Discussion

### 3.1 Pressure effect on resistance anomalies

The temperature dependence of the interlayer resistance under pressure reported in Ref. 40 is reproduced in Fig. 2. At 0 kbar, three hump anomalies are clearly observed. The inset shows the temperature dependence of  $dR/dT$  at 0 kbar. Three resistance anomalies at  $T_1 = 174$  K,  $T_2 = 72$  K, and  $T_3 = 22$  K are indicated by the arrows. At 2.0 kbar, the anomalies at  $T_2$  and  $T_3$  are slightly shifted to lower temperatures, while the anomaly at  $T_1$  is completely absent. The significant increase in resistance with decreasing temperature below room temperature at 2.0 kbar shows that  $T_1$  is higher than room temperature. Since it is reported that the CO state in the ET layers disappears below  $T_1$ ,<sup>33</sup> we can conclude that there is no CO state below room temperature at 2.0 kbar. At 5.1 kbar, the  $T_3$ -anomaly is not observed and only the  $T_2$ -anomaly is still observed. The absence of the  $T_3$ -anomaly shows that there is no nesting of the pair of warped 1D FSs originating from the ET bands. Thus, we found that the electronic state of  $\beta''$ -(ET)(TCNQ) is drastically changed by the application of pressure.

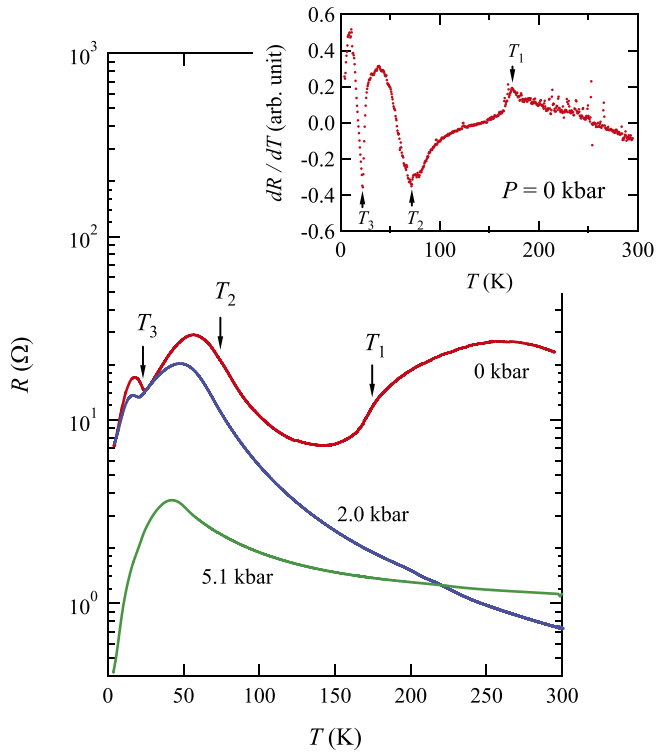


**Fig. 2.** (Color online) Resistance of  $\beta''$ -(ET)(TCNQ) as a function of temperature under three pressures.<sup>40)</sup> The inset shows the temperature dependence of  $dR/dT$  at  $P = 0$  kbar. Three resistance anomalies at  $T_1$ ,  $T_2$ , and  $T_3$  are indicated by the arrows.

Although the origin of the  $T_2$ -anomaly is still unclear, the semiconductor-like behavior below  $T_1$  at 0 kbar or below room temperature under pressures may be associated with a possible  $4k_F$ -CDW gap. According to the optical conductivity measurement,<sup>33)</sup> the CO state in the ET layers collapses and bad metal (or charge disproportionation) with incoherent electron transport appears below  $T_1$ . Interestingly, the electron transport in the ET layers shows a crossover behavior into a coherent Fermi liquid state below  $T_2$  [Note that  $T_2$  is defined as an inflection point in each  $R(T)$  curve in

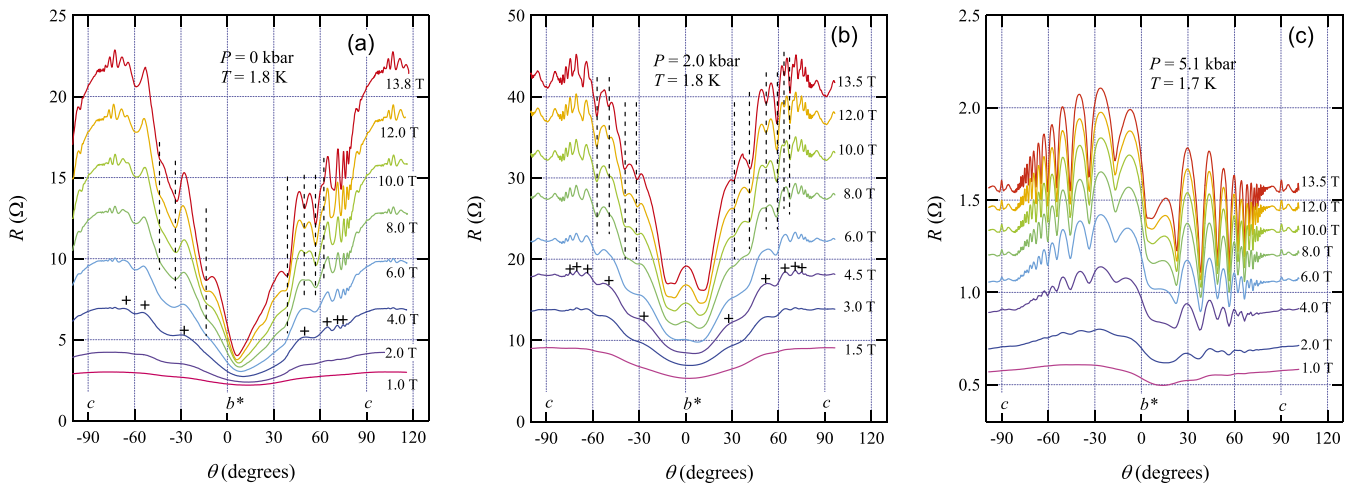
Fig. 2]. Thus, the  $T_2$ -anomaly represents not a thermodynamic phase transition but the crossover behavior. The absence of the anomalies in the magnetic susceptibility around  $T_2$ <sup>31)</sup> is consistent with the above discussion. The temperature–pressure phase diagram for  $\beta''$ -(ET)(TCNQ) is discussed later.

### 3.2 Angular-dependent magnetoresistance

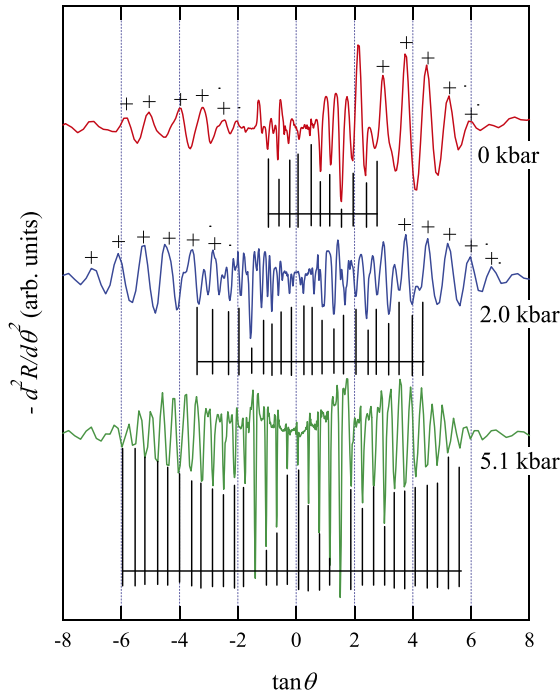
Figure 3(a) shows the  $\theta$ -dependence of the interlayer resistance in magnetic fields rotated on the  $b^*$ - $c$  plane. As pointed out previously,<sup>27)</sup> the oscillatory behavior consists of the resistance peaks due to the Yamaji oscillation and the dips due to the commensurability effect at ambient pressure. As shown in Fig. 3(a), the Yamaji oscillation, marked by crosses, is dominantly observed at 4.0 T. This oscillation arises from the small pocket created by the imperfect nesting of the FSs originating from the ET layers.<sup>27,37)</sup> Above 10 T, the dip structure is superimposed, as indicated by the dashed lines. With increasing magnetic field, the dip structures become sharper, and their positions are independent of the magnetic field strength. The results clearly show that the dips are not caused by quantum oscillation but by the commensurability effect.<sup>38)</sup> Similar dips due to the commensurability effect are observed in a DW phase of  $\alpha$ -(ET)<sub>2</sub>MHg(SCN)<sub>4</sub> ( $M = K, Rb, Tl$ ).<sup>42–44)</sup>

Figure 3(b) shows the  $\theta$ -dependence of the interlayer resistance at 2.0 kbar, where  $T_1$  is probably higher than room temperature. The oscillatory behavior at 2.0 kbar is very similar to that at 0 kbar, suggesting no significant change in electronic structure at 2.0 kbar. At around  $\theta = 0^\circ$ , a new hump forms above 6.0 T and becomes distinct with increasing magnetic field. A similar hump has been reported in an organic superconductor with an incommensurate superlattice potential<sup>45)</sup> and a high- $T_c$  cuprate superconductor.<sup>46)</sup> The humps have been discussed in terms of  $p$ -type or  $d_{xy}$ -type staggered warping in the 2D FSs.<sup>47)</sup> Such staggered warping in the 2D FSs will likely be induced by applying pressure in  $\beta''$ -(ET)(TCNQ).

Figure 3(c) shows the results obtained at 5.1 kbar, where only the  $T_2$ -anomaly is observed. Many sharp dips, whose positions are independent of the magnetic field strength, are



**Fig. 3.** (Color online) Angular-dependent magnetoresistance of  $\beta''$ -(ET)(TCNQ) for various magnetic fields under various pressures: (a)  $P = 0$  kbar, (b)  $P = 2.0$  kbar, and (c)  $P = 5.1$  kbar. In (a) and (b), the crosses and dashed lines show peaks of Yamaji oscillation and dips due to the commensurability effect, respectively. The positions of peaks and dips are independent of applied magnetic field.



**Fig. 4.** (Color online) Second-derivative curves of magnetoresistance as a function of  $\tan \theta$  at 13.8 T for 0 kbar and at 13.5 T for 2.0 and 5.1 kbar. Both peaks (crosses) and dips (lines) are visible at 0 and 2.0 kbar, although only dips are observed at 5.1 kbar. All peaks and dips are periodic in  $\tan \theta$ .

observed. The dips will be attributable to the commensurability effect, as observed in Figs. 3(a) and 3(b). No Yamaji oscillations are observed. In addition, the peak at  $\theta = \pm 90^\circ$  is evident at high fields, showing coherent interlayer transport.<sup>48,49</sup> The pressure effect on the resistance peak at  $\theta = \pm 90^\circ$  is discussed later.

To see the oscillations more clearly, we plot the second derivative curves of the magnetoresistance as a function of  $\tan \theta$  at three pressures in Fig. 4. At 0 and 2.0 kbar, the dips with a short period are evident in a low-angle region, whereas the peaks with a long period are observed more clearly in a high-angle region. Both dips and peaks are periodic in  $\tan \theta$ . The observation of the dips and peaks clearly shows that the DW from the ET band or the possible  $4k_F$ -CDW from the TCNQ band coexists with a 2D pocket at 2.0 kbar below  $T_3$ ; the electronic structure at 2.0 kbar is essentially the same as that at ambient pressure.

At 5.1 kbar, the peaks disappear and only the dips are visible. Since the peaks (Yamaji oscillation) are ascribed to the  $\alpha$ -orbit generated by the imperfect nesting of the FSs on the ET layers, the absence of the peaks shows no FS nesting at 5.1 kbar: the DW state on the ET layers is totally suppressed. On the other hand, the  $T_2$ -anomaly is still observed, as seen in Fig. 2. Therefore, we conclude that the dip structure is attributable not to the DW state on the ET layers but to the possible  $4k_F$ -CDW phase in the TCNQ band.

Note that the sharp dip structure in the angular-dependent magnetoresistance was reported in Ref. 40, where the mechanism of the dip structure was discussed in terms of a 1D FS with higher order corrugation, whose model is theoretically discussed by Blundell and Singleton.<sup>50</sup> An explanation based on the 1D FS scenario was not entirely convincing because it required an unphysical long-range

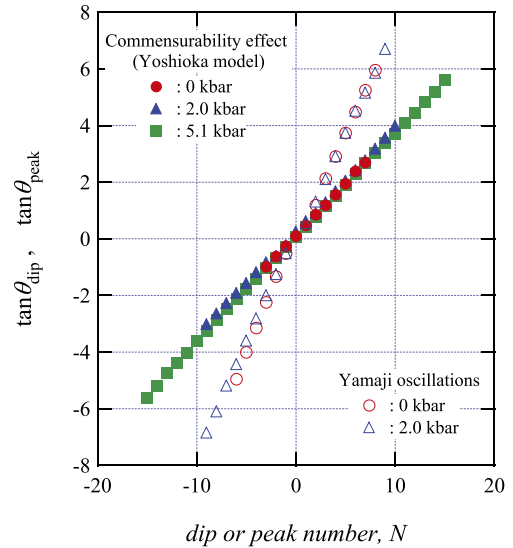


**Fig. 5.** (Color online) Plots of  $\tan \theta_{\text{dip}}$  and  $\tan \theta_{\text{peak}}$  versus  $N$  (dip or peak number), where  $\theta_{\text{dip}}$  and  $\theta_{\text{peak}}$  are the dip and peak angles, respectively, obtained from Figs. 3 and 4.

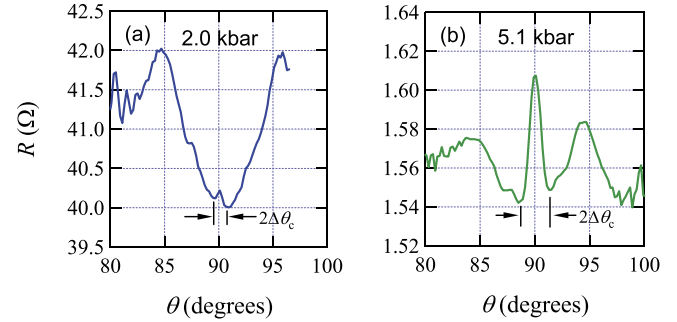


**Fig. 6.** (Color online) Enlarged views of Figs. 3(b) and 3(c) at 13.5 T around  $\theta = 90^\circ$  for (a)  $P = 2.0$  kbar and (b)  $P = 5.1$  kbar, respectively.

transfer integral between the ET chains parallel to the  $a$ -axis.<sup>40</sup>

Figure 5 shows the plots of  $\tan \theta_{\text{dip}}$  and  $\tan \theta_{\text{peak}}$  versus  $N$  (dip or peak number), where  $\theta_{\text{dip}}$  and  $\theta_{\text{peak}}$ , obtained from Figs. 3 and 4, represent the angles of dips and peaks, respectively. The slopes in these plots correspond to the periods of the dip and peak with respect to  $\tan \theta$ . As can be seen in Fig. 5, there is no significant change in dip period under pressure, indicating that the superlattice in the possible  $4k_F$ -CDW phase is almost unchanged under pressure. The periodicity  $\Delta$  of the peaks associated with the Yamaji oscillation as a function of  $\tan \theta$  is given by  $\Delta = \pi / (dk_F)$ ,<sup>24</sup> where  $d$  ( $= 20.36 \text{ \AA}$ ) is the interlayer spacing and  $k_F$  is the Fermi wave number. From the slope of  $\tan \theta$  associated with the peak positions versus  $N$ , the periodicity  $\Delta$  is obtained and then  $k_F$  is estimated to be  $0.182 \pm 0.010 \text{ \AA}^{-1}$  at 0 kbar and  $0.199 \pm 0.004 \text{ \AA}^{-1}$  at 2.0 kbar. Although the shape of the  $\alpha$ -orbit at 2.0 kbar is unknown, we expect that a similar nesting of the FSs from the ET bands occurs down to 2.0 kbar.

Let us discuss the peak effect appearing at  $\theta = \pm 90^\circ$  for  $P = 2.0$  kbar. Figure 6(a) shows the enlarged view of Fig. 3(b) at 13.5 T around  $\theta = 90^\circ$ , where a small peak can be seen. Such a peak, as observed in various low-dimensional conductors, is known to result from the closed orbits on the

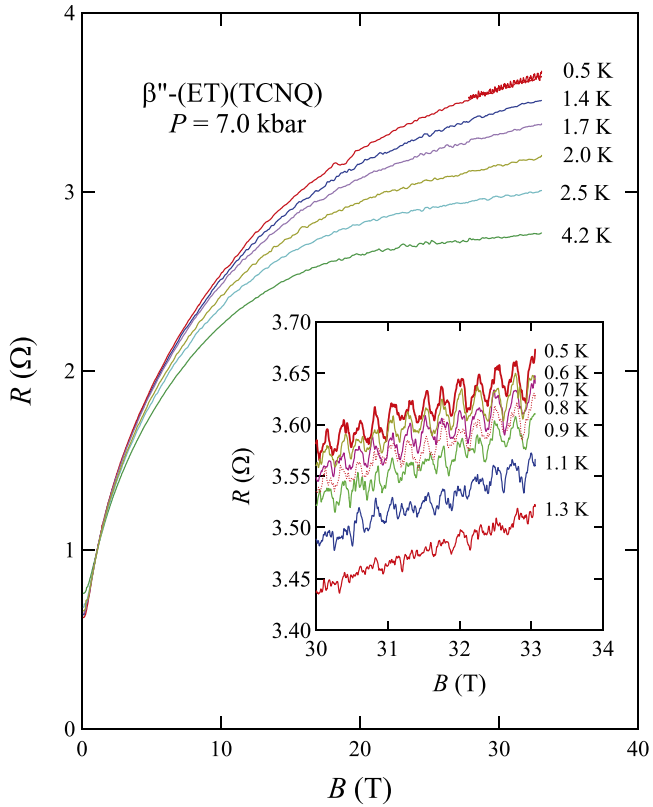


**Fig. 7.** (Color online) Interlayer resistance of  $\beta''$ -(ET)(TCNQ) as a function of magnetic field at various temperatures ranging from 0.5 to 4.2 K. The inset is the interlayer resistance for the high-field range between 30 and 33 T below 1.3 K, where high-frequency SdH oscillations are found.

side of the warped 1D or cylindrical 2D FS.<sup>48,49</sup> The peak provides evidence for coherent interlayer transport in the layered systems.<sup>48,49</sup> The width of the peak is proportional to the interlayer transfer integral.<sup>48,49</sup> From Fig. 6(a), the peak width  $2\Delta\theta_c$  is estimated to be  $0.8^\circ$ , which is nearly equal to that at ambient pressure.<sup>27</sup> Since the magnetic field is rotated on the  $b^*-c$  plane, the peak will be ascribed to the small closed orbit on the long-axis side of the cross section of the corrugated cylindrical FS related to the  $\alpha$ -orbit.<sup>27</sup>

Next, we discuss the peak effect for  $P = 5.1$  kbar. Figure 6(b) shows the enlarged view of Fig. 3(c) at 13.5 T around  $\theta = 90^\circ$ . Compared with the resistance peak at 2.0 kbar, the width of the resistance peak is markedly enhanced at 5.1 kbar. Since the resistance peak at 2.0 kbar is associated with the small pocket created by the nesting of the FSs originating from the ET layers, it is likely that the enhanced peak structure at 5.1 kbar is caused by the corrugation of the warped 1D FSs formed by the ET band. From Fig. 6(b), the peak width  $2\Delta\theta_c$  is estimated to be  $2.8^\circ$ , which is three times larger than that at ambient pressure and 2.0 kbar. This result suggests a significant enhancement of the interlayer transfer integral and corrugation of the FS formed by the ET band at 5.1 kbar.

### 3.3 Shubnikov–de Haas effect

Figure 7 shows the magnetic field dependence of the interlayer resistance over a temperature range from 0.5 to 4.2 K at 7.0 kbar. The interlayer resistance increases with magnetic field strength. The SdH oscillation resulting from the  $\alpha$ -orbit with the frequency of 137 T is observed at

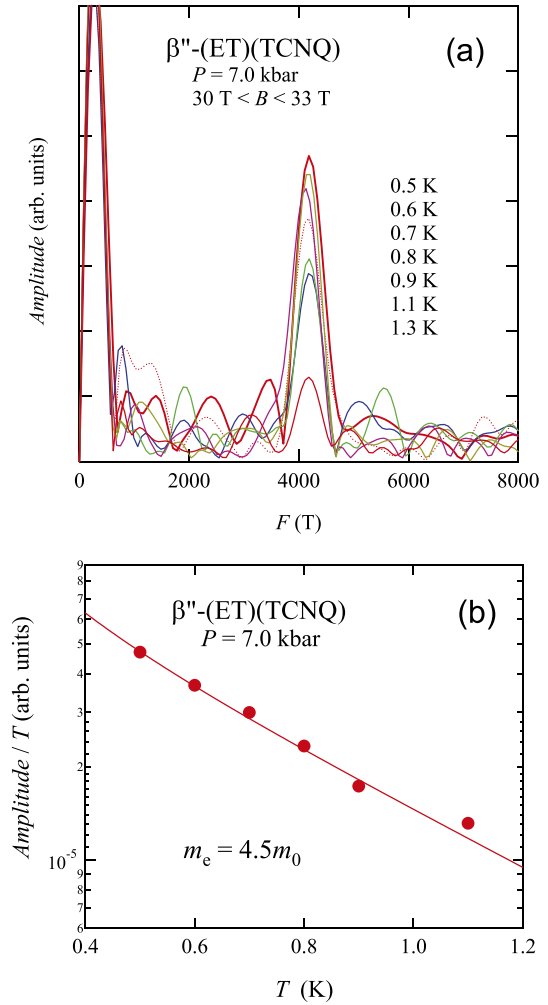


**Fig. 8.** (Color online) (a) Fourier transform spectra of the SdH oscillations at 7.0 kbar. (b) Fourier transform spectrum amplitude divided by temperature versus temperature (mass plot). A solid curve is the result calculated using the Lifshitz–Kosevich formula.

0 kbar.<sup>27</sup> In contrast, as shown in the inset of Fig. 7, high-frequency SdH oscillations above 30 T are evident at 7.0 kbar.

Figure 8(a) shows the Fourier transform spectrum of the SdH oscillations in the magnetic field range of 30 to 33 T. The high frequency of 4183 T indicates that the cross-sectional area of the FS is approximately 30% of the first Brillouin zone. The Fourier transform amplitude divided by temperature plotted against temperature, called the mass plot, is shown in Fig. 8(b). A solid curve is the result calculated using the Lifshitz–Kosevich formula.<sup>19</sup> The numerical fit of the data provides the effective mass of  $m_e = 4.5m_0$ , where  $m_0$  is the free electron mass. This effective mass is about four times larger than that in the  $\alpha$ -pocket at 0 kbar. The observation of a larger FS with a heavier effective mass indicates a significant difference between the FSs at 0 and 7.0 kbar. The observations of the dip structure [Fig. 3(c)] and the  $T_2$ -anomaly in  $R(T)$  show the existence of the possible  $4k_F$ -CDW and the absence of the FS originating from the TCNQ layers at 7.0 kbar. Therefore, the ET-derived FSs are responsible for the high-frequency SdH oscillations. It is likely that the transfer integral along the  $c$ -axis increases with pressure, leading to a significant undulation of the FSs originating from the ET layers. The lack of Yamaji oscillation

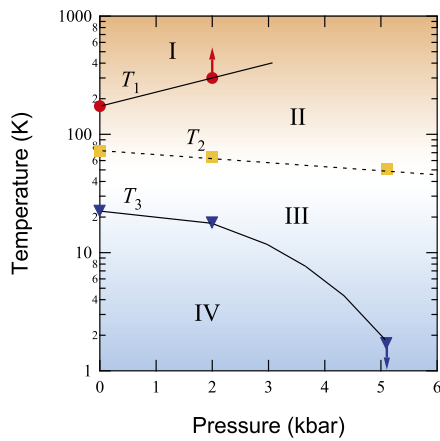


**Fig. 9.** (Color online)  $T$ - $P$  phase diagram of  $\beta''$ -(ET)(TCNQ) derived from Fig. 2. At 2.0 kbar, the  $T_1$ -anomaly may occur at a temperature above room temperature. A critical pressure for the DW phase, where  $T_3$  goes to zero, is estimated to be  $\sim 5$  kbar. The dashed line dividing regions II and III means the pressure dependence of  $T_2$ , where the bad metal with incoherent electron transport shows a crossover behavior into a coherent Fermi liquid state with decreasing temperature. See Sect. 3.4 for the electronic states in regions I, II, III, and IV.

at 5.1 kbar in Figs. 3(c) and 4 shows that the undulated FSs are not yet closed. Thus, a magnetic breakdown effect may play a crucial role in the observation of the SdH oscillations, that was not recognized in the previous SdH study.<sup>39</sup> The observation of the large effective mass of  $m_e = 4.5m_0$  suggests a mass enhancement by the strong electron correlation in the ET band, which is a source of the CO state in the ET layers.

### 3.4 $T$ - $P$ phase diagram

Figure 9 shows the  $T$ - $P$  phase diagram of  $\beta''$ -(ET)(TCNQ), derived from the resistance measurements (Fig. 2). There are four temperature regions, I ( $T > T_1$ ), II ( $T_1 > T > T_2$ ), III ( $T_2 > T > T_3$ ), and IV ( $T < T_3$ ), as previously defined and discussed at 0 kbar by Uruichi et al.<sup>33</sup> In region I, the CO state in the ET layers coexists with the possible  $4k_F$ -CDW in the TCNQ layers. In region II, the CO state in the ET layers collapses and the bad metal (or the charge disproportionation) with incoherent electron transport appears. According to the optical conductivity measurements,<sup>33</sup> the incoherent transport in the ET layers shows a crossover behavior into a coherent Fermi liquid state across  $T_2$  with decreasing temperature. In region III, the coherence of the quasiparticles in the ET layers grows monotonically with decreasing temperature. In region IV, the DW phase is formed in the ET layers and coexists with the possible  $4k_F$ -CDW in the TCNQ layers. In this region, small FS pockets are formed by the imperfect nesting of the FSs originating from the ET layers. A critical pressure for the DW phase, where  $T_3$  goes to zero, is estimated to be  $\sim 5$  kbar. Thus, we consider that the ground state above 5 kbar is the possible  $4k_F$ -CDW, where the 1D FSs originating from the ET layers are strongly undulated.

Finally, let us discuss the similarities and differences between the pressure-induced changes of  $\beta''$ -(ET)(TCNQ) and other organic conductors. As shown in Fig. 9,  $T_1$  increases with pressure. This behavior is completely different from the pressure effect on typical charge-ordered insula-

tors,<sup>51-53</sup> where a metal-insulator transition temperature accompanied by a CO state decreases with increasing pressure because of the enhanced electronic band overlap. The pressure dependence of the Raman spectra at room temperature showed that the pressure has the same effect as lowering the temperature, i.e., the thermal contraction of the lattice.<sup>33</sup> Therefore, lowering the temperature or increasing the pressure at around room temperature corresponds to a decrease in  $V/t$ , where  $V$  is the intersite Coulomb interaction and  $t$  is the intersite hopping energy, leading to the destabilization of the CO state and a resultant increase in  $T_1$  with pressure. As the temperature decreases across  $T_2$ , there is a crossover behavior from incoherent to coherent transport in the ET layers.<sup>33</sup> This phenomenon is very similar to the crossover behavior from a high-temperature bad metal to a low-temperature Fermi liquid metal in half-filled band systems such as  $\kappa$ -(ET)<sub>2</sub>X, where X stands for monovalent anions.<sup>54,55</sup> On the lower temperature side,  $T_3$  decreases with increasing pressure and the DW state is completely suppressed at around 5 kbar. Similar pressure effects are reported for the SDW phase in the Bechgaard salts<sup>56,57</sup> and the CDW phase in the  $\alpha$ -(ET)<sub>2</sub>KHg(SCN)<sub>4</sub>.<sup>42,58</sup>

### 4. Summary

We have studied the effect of pressure on the resistance anomalies, the angular-dependent magnetoresistance, and the SdH effect for  $\beta''$ -(ET)(TCNQ). When the  $T_3$ -anomaly is observed, the Yamaji oscillations and the dips explained by the Yoshioka model are clearly observed. However, when the  $T_3$ -anomaly is completely suppressed at 5.1 kbar, the Yamaji oscillations simultaneously disappear, but the dips become more evident. Since the semiconductor-like behavior below  $T_1$  at 0 kbar or below room temperature under pressure survives at 5.1 kbar, it is likely that the sharp dips are attributable to the possible  $4k_F$ -CDW in the TCNQ layers. The observation of the high-frequency SdH oscillation with the heavier effective mass shows a significant difference between the FSs at 0 and 7.0 kbar. The high-frequency SdH oscillation likely results from the magnetic breakdown effect on the strongly undulated FS originating from the ET layers under high pressure. The experimental results reported here demonstrate that the measurement of angular-dependent magnetoresistance provides a powerful tool for investigating charge-ordered states, such as DW and  $4k_F$ -CDW states, as well as conventional 2D FS studies.

**Acknowledgments** The authors thank Professor M. Kimata, Professor K. Yakushi, Dr. K. Enomoto, and Dr. T. Kawamoto for their useful discussion and suggestion. The authors would like to thank Ms. M. Nishimura for her hearty cooperation in our experiments. This work was supported by World Premier International Research Center Initiative (WPI), MEXT, Japan. A portion of this work was performed at the National High Magnetic Field Laboratory, which is supported by National Science Foundation Cooperative Agreement Nos. DMR-1644779 and DMR-2128556 and the State of Florida.

\*yasuzuka@cc.it-hiroshima.ac.jp

<sup>†</sup>Deceased 27 September 2014

- 1) H. Fukuyama, *J. Phys. Soc. Jpn.* **75**, 051001 (2006).
- 2) S. Yasuzuka, H. Koga, Y. Yamamura, K. Saito, S. Uji, T. Terashima, H. Akutsu, and J. Yamada, *J. Phys. Soc. Jpn.* **86**, 084704 (2017).
- 3) S. Yasuzuka, *Crystals* **11**, 600 (2021).
- 4) S. Yasuzuka, K. Saito, S. Uji, M. Kimata, H. Satsukawa, T. Terashima,

- and J. Yamada, *J. Phys. Soc. Jpn.* **82**, 064716 (2013).
- 5) S. Yasuzuka, S. Uji, T. Terashima, K. Sugii, B. Zhou, A. Kobayashi, and H. Kobayashi, *J. Phys. Soc. Jpn.* **83**, 013705 (2014).
  - 6) S. Yasuzuka, S. Uji, T. Terashima, K. Sugii, T. Isono, Y. Iida, and J. A. Schlueter, *J. Phys. Soc. Jpn.* **84**, 094709 (2015).
  - 7) K. Murata, S. Kagoshima, S. Yasuzuka, H. Yoshino, and R. Kondo, *J. Phys. Soc. Jpn.* **75**, 051015 (2006).
  - 8) S. Yasuzuka and K. Murata, *Sci. Technol. Adv. Mater.* **10**, 024307 (2009).
  - 9) S. Yasuzuka, Y. Okajima, S. Tanda, K. Yamaya, N. Takeshita, and N. Mōri, *Phys. Rev. B* **60**, 4406 (1999).
  - 10) S. Yasuzuka, Y. Okajima, S. Tanda, N. Takeshita, N. Mōri, and K. Yamaya, *J. Phys. Soc. Jpn.* **69**, 3470 (2000).
  - 11) S. Yasuzuka, S. Uji, S. Sugiura, T. Terashima, Y. Nogami, K. Ichimura, and S. Tanda, *J. Supercond. Novel Magn.* **33**, 953 (2020).
  - 12) S. Yasuzuka, K. Murata, T. Fujimoto, M. Shimotori, and K. Yamaya, *J. Phys. Soc. Jpn.* **74**, 1782 (2005).
  - 13) S. Yasuzuka, K. Yamaya, Y. Okajima, S. Tanda, N. Takeshita, H. Mitamura, T. Nakanishi, and N. Mōri, *J. Phys. Soc. Jpn.* **74**, 1787 (2005).
  - 14) S. Yasuzuka, K. Murata, H. Yoshino, T. Fujimoto, M. Shimotori, M. Nakamura, and M. Tadokoro, *J. Phys. Soc. Jpn.* **75**, 014704 (2006).
  - 15) S. Yasuzuka, K. Murata, M. Shimotori, T. Fujimoto, J. Yamada, and K. Kikuchi, *J. Phys. Soc. Jpn.* **75**, 024701 (2006).
  - 16) S. Yasuzuka, K. Murata, T. Fujimoto, M. Shimotori, T. Kawamoto, T. Mori, M. Hedo, and Y. Uwatoko, *J. Phys. Soc. Jpn.* **75**, 053701 (2006).
  - 17) S. Yasuzuka, K. Kobayashi, H. Nishikawa, H. Yoshino, and K. Murata, *J. Phys. Soc. Jpn.* **75**, 083710 (2006).
  - 18) S. Yasuzuka, K. Murata, T. Arimoto, and R. Kato, *J. Phys. Soc. Jpn.* **76**, 033701 (2007).
  - 19) D. Shoenberg, *Magnetic Oscillations in Metals* (Cambridge University Press, Cambridge, U.K., 1984).
  - 20) J. Wosnitzer, *Fermi Surfaces of Low-Dimensional Organic Metals and Superconductors* (Springer, Berlin, 1996).
  - 21) K. Kajita, Y. Nishio, T. Takahashi, W. Sasaki, R. Kato, H. Kobayashi, and A. Kobayashi, *Solid State Commun.* **70**, 1181 (1989).
  - 22) K. Kajita, Y. Nishio, T. Takahashi, W. Sasaki, H. Kobayashi, A. Kobayashi, R. Kato, and Y. Iye, *Synth. Met.* **42**, 2075 (1991).
  - 23) M. V. Kartsovnik, P. A. Kononovich, V. N. Laukhin, and I. F. Schegolev, *Pis'ma Z. Eksp. Teor. Fiz.* **48**, 498 (1988) [in Russian].
  - 24) K. Yamaji, *J. Phys. Soc. Jpn.* **58**, 1520 (1989).
  - 25) S. Yasuzuka, S. Uji, H. M. Yamamoto, J.-I. Yamaura, C. Terakura, T. Terashima, T. Yakabe, Y. Terai, R. Maeda, and R. Kato, *J. Phys. Soc. Jpn.* **74**, 679 (2005).
  - 26) S. Yasuzuka, H. Koga, Y. Yamamura, K. Saito, S. Uji, T. Terashima, H. Aizawa, K. Kuroki, M. Tsuchiizu, H. Akutsu, and J.-I. Yamada, *J. Phys. Soc. Jpn.* **81**, 035006 (2012).
  - 27) S. Yasuzuka, S. Uji, T. Konoike, T. Terashima, D. Graf, E. S. Choi, J. S. Brooks, H. M. Yamamoto, and R. Kato, *J. Phys. Soc. Jpn.* **85**, 084701 (2016).
  - 28) H. Ohta, M. Kimata, and Y. Oshima, *Sci. Technol. Adv. Mater.* **10**, 024310 (2009).
  - 29) T. Kiss, A. Chainani, H. M. Yamamoto, T. Miyazaki, T. Akimoto, T. Shimojima, K. Ishizaka, S. Watanabe, C.-T. Chen, A. Fukaya, R. Kato, and S. Shin, *Nat. Commun.* **3**, 1089 (2012).
  - 30) H. M. Yamamoto, M. Hagiwara, and R. Kato, *Synth. Met.* **133–134**, 449 (2003).
  - 31) H. M. Yamamoto, N. Tajima, M. Hagiwara, R. Kato, and J.-I. Yamaura, *Synth. Met.* **135–136**, 623 (2003).
  - 32) K. Yakushi, M. Uruichi, H. M. Yamamoto, and R. Kato, *J. Phys. IV France* **114**, 149 (2004).
  - 33) M. Uruichi, K. Yakushi, H. M. Yamamoto, and R. Kato, *J. Phys. Soc. Jpn.* **75**, 074720 (2006).
  - 34) K. Yakushi, *Crystals* **2**, 1291 (2012).
  - 35) M. Ogura, N. Hanasaki, Y. Nogami, K. Yakushi, H. M. Yamamoto, and R. Kato, private communication.
  - 36) S. Yasuzuka, C. Terakura, T. Terashima, T. Yakabe, Y. Terai, H. M. Yamamoto, R. Kato, and S. Uji, *Synth. Met.* **135–136**, 647 (2003).
  - 37) M. Kimata, Y. Oshima, H. Ohta, K. Koyama, M. Motokawa, H. M. Yamamoto, and R. Kato, *Phys. Rev. B* **75**, 045126 (2007).
  - 38) D. Yoshioka, *J. Phys. Soc. Jpn.* **64**, 3168 (1995).
  - 39) S. Yasuzuka, D. Graf, E. S. Choi, J. S. Brooks, T. Terashima, T. Konoike, K. Enomoto, M. Nishimura, H. M. Yamamoto, R. Kato, and S. Uji, *J. Phys. IV* **114**, 157 (2004).
  - 40) S. Yasuzuka, S. Uji, K. Enomoto, T. Konoike, M. Nishimura, T. Terashima, D. Graf, E. S. Choi, J. S. Brooks, H. M. Yamamoto, R. Kato, K. Yokogawa, and K. Murata, *Synth. Met.* **152**, 437 (2005).
  - 41) K. Murata, H. Yoshino, H. O. Yadav, Y. Honda, and N. Shirakawa, *Rev. Sci. Instrum.* **68**, 2490 (1997).
  - 42) N. Hanasaki, S. Kagoshima, N. Miura, and G. Saito, *J. Phys. Soc. Jpn.* **65**, 1010 (1996).
  - 43) K. Uchida, R. Yamaguchi, T. Konoike, T. Osada, and W. Kang, *J. Phys. Soc. Jpn.* **82**, 043714 (2013).
  - 44) W. Kang, T. Osada, T. Konoike, and K. Uchida, *Phys. Rev. B* **88**, 195105 (2013).
  - 45) T. Kawamoto, T. Mori, K. Enomoto, T. Konoike, T. Terashima, S. Uji, A. Takamori, K. Takimiya, and T. Otsubo, *Phys. Rev. B* **73**, 024503 (2006).
  - 46) N. E. Hussey, M. Abdel-Jawad, A. Carrington, A. P. Mackenzie, and L. Balicas, *Nature (London)* **425**, 814 (2003).
  - 47) R. Yagi and Y. Iye, *Solid State Commun.* **89**, 275 (1994).
  - 48) N. Hanasaki, S. Kagoshima, T. Hasegawa, T. Osada, and N. Miura, *Phys. Rev. B* **57**, 1336 (1998).
  - 49) M. V. Kartsovnik, V. N. Laukhin, S. I. Pesotskii, I. F. Schegolev, and V. M. Yakovenko, *J. Phys. I France* **2**, 89 (1992).
  - 50) S. J. Blundell and J. Singleton, *Phys. Rev. B* **53**, 5609 (1996).
  - 51) T. Itou, K. Kanoda, K. Murata, T. Matsumoto, K. Hiraki, and T. Takahashi, *Phys. Rev. Lett.* **93**, 216408 (2004).
  - 52) H. Nishikawa, Y. Sato, K. Kikuchi, T. Kodama, I. Ikemoto, J. Yamada, H. Oshio, R. Kondo, and S. Kagoshima, *Phys. Rev. B* **72**, 052510 (2005).
  - 53) N. Tajima, M. Tamura, Y. Nishio, K. Kajita, and Y. Iye, *J. Phys. Soc. Jpn.* **69**, 543 (2000).
  - 54) P. Limelette, P. Wzietek, S. Florens, A. Georges, T. A. Costi, C. Pasquier, D. Jerome, C. Meziere, and P. Batail, *Phys. Rev. Lett.* **91**, 016401 (2003).
  - 55) J. Merino and R. H. McKenzie, *Phys. Rev. B* **61**, 7996 (2000).
  - 56) D. Jérôme, A. Mazaud, M. Ribault, and K. Bechgaard, *J. Phys. Lett. (France)* **41**, 95 (1980).
  - 57) K. Yamaji, *J. Phys. Soc. Jpn.* **51**, 2787 (1982).
  - 58) N. Hanasaki, S. Kagoshima, N. Miura, and G. Saito, *Phys. Rev. B* **63**, 245116 (2001).